

# RelTopo: Enhancing Relational Modeling for Driving Scene Topology Reasoning

Yueru Luo<sup>1,2</sup>, Changqing Zhou<sup>3</sup>, Yiming Yang<sup>1,2</sup>, Erlong Li<sup>4</sup>, Chao Zheng<sup>4</sup>,  
Shuqi Mei<sup>4</sup>, Shuguang Cui<sup>2,1</sup>, Zhen Li<sup>2,1\*</sup>

<sup>1</sup>FNii, Shenzhen; <sup>2</sup>SSE, CUHK-Shenzhen; <sup>3</sup>HKUST-Guangzhou; <sup>4</sup>Tencent Map T-Lab

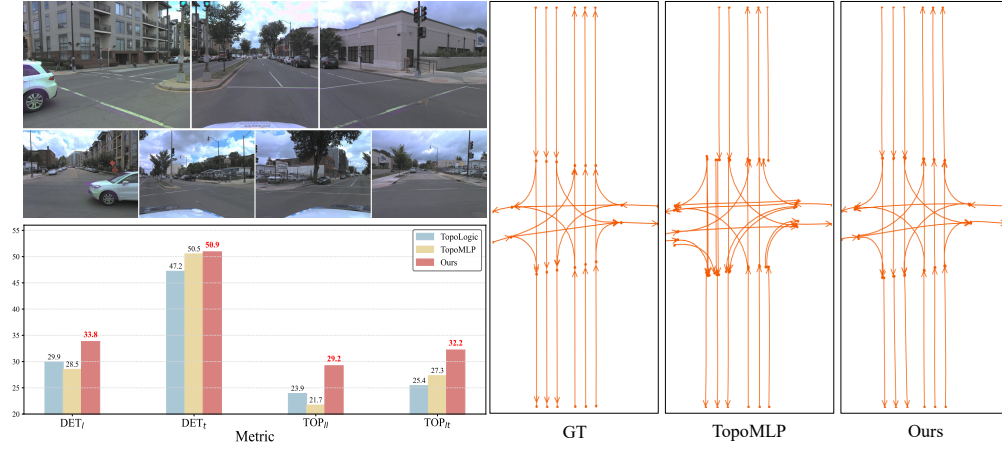


Figure 1: **Performance and visualization comparison between previous methods and ours.** The top-left multi-view images represent the model inputs. Our method, which models hybrid relations among lanes and cross-relations between lanes and traffic elements, demonstrates enhanced perception and reasoning capabilities, as illustrated in the visualizations on the right. Evaluated on the OpenLane-V2 dataset, **our model** significantly outperforms previous approaches across all metrics.

## Abstract

Accurate road topology reasoning is critical for autonomous driving, enabling effective navigation and adherence to traffic regulations. Central to this task are lane perception and topology reasoning. However, existing methods typically focus on either lane detection or Lane-to-Lane (L2L) topology reasoning, often *neglecting* Lane-to-Traffic-element (L2T) relationships or *failing* to optimize these tasks jointly. Furthermore, most approaches either overlook relational modeling or apply it in a limited scope, despite the inherent spatial relationships among road elements. We argue that relational modeling is beneficial for both perception and reasoning, as humans naturally leverage contextual relationships for road element recognition and their connectivity inference. To this end, we introduce relational modeling into both perception and reasoning, *jointly* enhancing structural understanding. Specifically, we propose: 1) a relation-aware lane detector, where our geometry-biased self-attention and curve-guided cross-attention refine lane representations by capturing relational dependencies; 2) relation-enhanced topology heads, including a geometry-enhanced L2L head and a cross-view L2T head, boosting reasoning with relational cues; and 3) a contrastive learning strategy with InfoNCE loss to regularize relationship embeddings. Extensive experiments on OpenLane-V2 demonstrate that our approach significantly improves both detection and topology

\*Corresponding Author

reasoning metrics, achieving +3.1 in  $DET_l$ , +5.3 in  $TOP_{ll}$ , +4.9 in  $TOP_{lt}$ , and an overall +4.4 in OLS, setting a new state-of-the-art. Code will be released.

## 1 Introduction

Understanding road topology is essential for safe and effective autonomous driving, as it provides vehicles with crucial spatial and contextual information for navigation. A comprehensive topology model requires reasoning over lane-to-lane (L2L) and lane-to-traffic-element (L2T) relationships, enabling autonomous vehicles to follow traffic regulations and execute safe maneuvers. This task involves two key components: 1) Perception, which detects lanes and traffic elements (*e.g.*, traffic lights) detection, with lane perception distinct from general objects. and 2) Reasoning, which infers L2L and L2T relationships to construct a structured representation of road topology.

**Lane Perception.** Most existing methods [1, 2, 3] adapt generic object detectors [4, 5] for lane perception by modifying bounding box into lane points or parametric representations. However, these adaptations often overlook [1, 2, 6] the *intrinsic geometric relationships* [7, 8] among lanes (*e.g.*, parallelism and connectivity), which humans naturally leverage for lane perception. TopoLogic [3] partially addresses this by introducing a geometry distance topology, which maps end-to-start point distances to connectivity labels (connected vs. non-connected) and integrates this information into lane feature learning via a Graph Neural Network (GNN). However, it focuses solely on connectivity and requires additional GNN to encode these relationships into lane features. It remains an open problem: *How can we effectively integrate inherent structural relationships in road scenes to enhance lane perception and topology reasoning?*

**Topology Reasoning.** For **L2L reasoning**, existing methods [2, 6, 9] enhance lane features using coordinate-based encoding but are highly sensitive to endpoint shifts, causing errors [3]. TopoLogic [3] partially addresses this with geometric distance topology, applied both within the model and as post-processing. Our experiments (*Supp. Tab. 3*) show that removing this post-processing significantly degrades their L2L performance, indicating that the model fails to learn robust relational features. This raises a key question: *Can we achieve L2L reasoning end-to-end without relying on post-processing?* For **L2T reasoning**, which remains largely underexplored, current methods often model L2T relationships by naively combining BEV lane features with Front View (FV) traffic element features, ignoring the spatial discrepancy between these spaces. Topo2D [9] mitigates this issue by leveraging 2D lane features from an additional decoder, but adds computational overhead.

Our key insight is that **relational modeling is crucial for both lane perception and topology reasoning, yet remains underexplored**. To address this, we introduce explicit relational modeling for both tasks: In **lane perception**, we adopt a compact Bézier curve representation and design a relation-aware lane decoder with two key components: 1) Geometry-Biased Self-Attention (GBSA), which encodes inter-lane geometric relationships as attention biases, capturing spatial structures like parallelism and connectivity; and 2) Curve-Guided Cross-Attention (CGCA), which aggregates long-range context along lanes to enhance their representations. While the Bézier representation is compact and flexible [10], its sparse control points pose challenges for feature extraction, particularly for elongated or curved lanes (Fig. 3). We overcome this by leveraging on-curve relational cues to enhance lane representation learning (Sec. 3.2.2).

In **topology reasoning**, we introduce two specialized modules: 1) Geometry-Enhanced L2L reasoning module, which encodes inter-lane distance into high-dimensional features, improving L2L connectivity predictions and reducing sensitivity to minor perception errors; 2) Cross-View (X-view) L2T reasoning module, which bridges BEV lanes and FV traffic elements through a cross-view fusion design, aligning BEV lane features with FV traffic elements and enriching their representations with dual-view (BEV and FV) information. This design enables more robust L2T topology reasoning, as validated in our experiments. 3) To further enhance relation learning, we introduce a **contrastive learning** strategy, inspired by InfoNCE [11, 12, 13], to enhance the model’s ability in distinguishing connected (positive) and non-connected (negative) pairs for both L2L and L2T reasoning.

Overall, our contributions can be summarized as follows:

- We identify the limited exploration of relational modeling in existing methods and propose a **relation-aware lane decoder** with geometry-biased self-attention for inter-lane geometric relationships and curve-guided cross-attention for contextual information aggregation.

- We introduce **two topology reasoning modules**: a geometry-enhanced L2L module that captures inter-lane relationships with encoded geometry embeddings, and a X-view L2T module bridges BEV and FV features for enhanced L2T reasoning. To further enhance relational reasoning, we integrate a novel **contrastive learning** strategy.
- Extensive experiments on the OpenLaneV2 dataset validate the effectiveness of our approach, surpassing previous methods across both detection and topology reasoning metrics.

## 2 Related Work

### 2.1 3D Lane Detection

3D lane detection is essential for accurately perceiving lane geometries in real-world traffic scenes. Recent research primarily focuses on extracting 3D lane features from *monocular* front-view images and can be broadly categorized into BEV-based and front-view-based approaches. BEV-based methods employ inverse perspective mapping (IPM) to transform front-view images into the BEV perspective, facilitating lane prediction [14, 15, 16, 17, 18, 7]. However, IPM-based methods suffer from distortions on non-flat roads due to their planar assumption, complicating lane detection in dynamic environments. To mitigate these limitations, front-view-based methods predict 3D lanes directly from FV image features, avoiding view transformation distortions. Recent approaches [19, 20, 21] employ query-based detectors [22, 5] directly on FV features, modeling 3D lane information without IPM and achieving improved performance. In our work, we extend lane perception to broader environments by leveraging multi-view images.

### 2.2 Online HD Map Construction

Online HD map construction aims to dynamically generate detailed road environment maps. Early methods, such as HDMaNet [23], use dense segmentation predictions with heuristic post-processing to vectorize map elements. VectorMapNet [24] improves upon this by adopting an end-to-end detection-and-serialization pipeline for generating map polylines. Subsequent studies enhance end-to-end HD map construction [25, 26, 27, 28, 29, 30, 8, 31, 32]. MapTR [25] adopts a DETR [22] framework with hierarchical query embeddings for map encoding. BeMapNet [27] and PivotNet [28] employ piecewise Bézier curves and dynamic point-based representations, respectively. InstaGraM [29] formulates map element generation as a graph problem utilizing a GNN-based framework. GeMap [8] learns HD map structures by modeling element shapes and relational properties. But it focus on individual instance geometry modeling, do not explicitly capture topology relationships among lanes, and relies on polyline representations with equidistant points, which lack flexibility and precision [28, 33] for nuanced lane description. To improve computational efficiency, various decoupled self-attention mechanisms [26, 32, 8] have been proposed for integrating intra-/inter-instance information. However, topology reasoning among elements are limited in this area.

### 2.3 Driving Scene Topology Reasoning

Early efforts in topology reasoning focused on lane connectivity. STSU [34] is among the first models to construct lane graphs in an end-to-end manner using BEV representations. Following this, TPLR [35] introduces minimal cycles to enforce topological consistency. While effective, these methods focus solely on lane perception using monocular images and lack interactions with traffic elements, which are critical for comprehensive scene understanding.

Recent approaches have extended topology reasoning to jointly model both L2L and L2T relationships, leveraging multi-view data for richer contextual understanding. TopoNet [1] introduces a GNN-based framework that enhances topology prediction through message passing between lane and traffic element embeddings. TopoMLP [2] adopts MLP-based topology heads for more efficient topology reasoning. LaneSegNet [36], built upon OpenLane V2 [37], introduces lane segments augmented with left and right-side lane lines and proposes lane segment attention to capture intra-lane dependencies. However, these methods do not explicitly model relationships between lanes or between lanes and traffic elements, limiting their ability to capture dependencies among these objects. Topo2D [9] incorporates 2D detections as priors to support 3D topology reasoning, while TopoLogic [3] combines geometry distance-based topology estimation with query similarity-based relational modeling via

GNNs. However, its geometry distance topology reasoning is applied as a post-processing step for L2L reasoning. RoadPainter [6] further refines point localization by utilizing BEV masks.

In contrast, we recognize that explicit relational modeling is critical for both perception and topology reasoning. Our approach integrates relational modeling into both perception and reasoning in an end-to-end manner, jointly enhancing lane detection and L2L and L2T topology reasoning capabilities.

### 3 Method

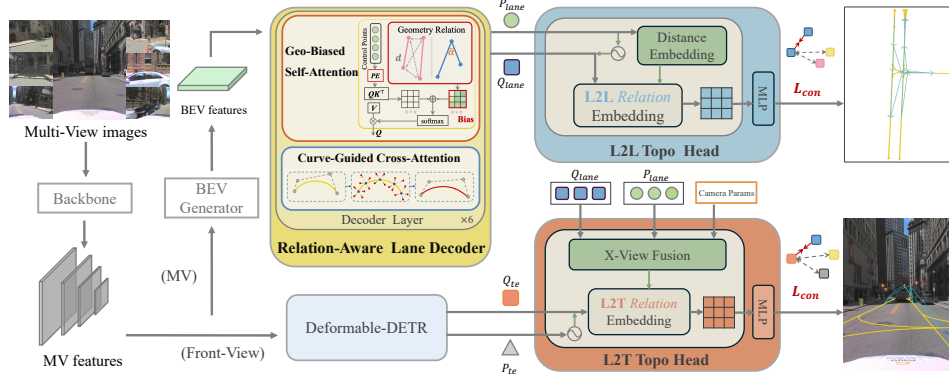


Figure 2: The overall framework of RelTopo, processing multi-view images with two main branches: (1) Lane branch projects multi-view image features to BEV space for lane centerline detection and lane-to-lane topology estimation; (2) Traffic elements branch detects traffic elements in front-view and infers lane-to-traffic-element relationships. Symbols  $\square$  ( $Q_{lane}$ ),  $\bullet$  ( $P_{lane}$ ),  $\square$  ( $Q_{te}$ ), and  $\triangle$  ( $P_{te}$ ) represent lane and traffic element queries with predicted outputs.  $L_{con}$  denotes our contrastive loss.

#### 3.1 Overview

As shown in Fig. 2, our model consists of two primary branches: the *Lane Branch* and the *Traffic Element Branch*. The Lane Branch features a **relation-aware lane decoder** (Sec. 3.2), which incorporates a geometry-biased self-attention to enable each lane to focus on geometrically related peers, enhancing its structural understanding. Additionally, we introduce a curve-guided cross-attention mechanism, which aggregates contextual features along the lane query with sampled points from the underlying curve. For L2L (Sec. 3.3) and L2T (Sec. 3.4) topology reasoning, we incorporate geometry-enhanced relation embeddings for L2L and X-view relation embeddings for L2T—to provide richer spatial context, improving the model’s ability to capture topological relationships. Furthermore, we introduce an additional contrastive loss (Sec. 3.5.2) to refine relation learning, enhancing the model’s ability to differentiate between various structural relationships.

#### 3.2 Relation-Aware Lane Decoder

To capture inter-lane geometric dependencies, we introduce a geometry-biased self-attention mechanism (Sec. 3.2.1) that enables the model to attend more effectively to spatially related lanes. Additionally, given the elongated and curved nature of lanes, we propose a curve-guided cross-attention mechanism (Sec. 3.2.2) to capture long-range contextual features along the lane path.

##### 3.2.1 Geometry-Biased Self-Attention

Learning effective query representations in DETR-like decoders can be slow and data-intensive [38, 39, 40]. [40] attributes this slow convergence to the lack of structural bias in query inputs and proposes a position relation module to accelerate the learning process. In lane perception, structurally related or connected lanes often share attributes, suggesting they can mutually enhance perception. Motivated by this, we propose a geometry-biased self-attention mechanism that encodes spatial relationships, such as inter-lane distances and angular differences, as attention biases. Unlike Topologic [3], which relies on GNNs to encode connectivity, we take a simpler yet effective approach by directly encoding geometric relationships as attention biases within self-attention. Additionally, we incorporate angular information for more comprehensive geometry relation modeling.



Formally, this mechanism is illustrated in Fig. 3, where ours  $\square$  is defined as Eq. (1), and  $\mathbf{Geometry}(l, l)_{(i,j)}$  represents the geometry bias term between  $i$ -th and  $j$ -th lanes.  $\text{Dist}(l_i, l_j)$  (minimum endpoint distance between lanes) and  $\text{Angle}(l_i, l_j)$  (angular difference) are concatenated and encoded through an embedding layer GE, which applies sinusoidal encoding followed by an MLP. This mechanism enhances query learning by introducing structural bias, as suggested in [40], while also improving the capture of inherent lane geometric relationships.

$$\mathbf{Q} = \text{Softmax} \left( \frac{\mathbf{Q}\mathbf{K}^\top}{\sqrt{d_{\text{model}}}} + \mathbf{Geometry}(l, l) \right) \mathbf{V} \quad (1)$$

$$\mathbf{Geometry}(l, l)_{(i,j)} = \text{GE}(\text{Dist}(l_i, l_j) \parallel \text{Angle}(l_i, l_j)), \quad (2)$$

By enhancing geometrically proximal lanes, it allows the model to allocate greater attention to spatially relevant lanes through the interleaved attention process, leading to a more robust understanding of lane topology (detailed in Sec. 3.3). Our method differs from TopoLogic [9], which uses end-to-start point distances and fails to capture relationships beyond connectivity, and from [40], which encodes progressive cross-layer box positional relationships for individual objects.

### 3.2.2 Curve-Guided Cross-Attention

Polyline representations with equidistant points often lack flexibility and precision [28, 33]. To overcome this limitation, we adopt a compact and flexible Bézier curve formulation, representing each lane as a third-degree Bézier curve defined by four control points. However, two challenges arise: 1) the sparsity of control points limits feature aggregation; 2) intermediate control points do not lie on the curve (green points in the right side of Fig. 3).

To address these issues, instead of relying solely on sparse control points as reference points in deformable attention like TopoDBA [41], we sample  $K$  points along the Bézier curve, which serves as reference points for feature aggregation (Fig. 3 right side). Furthermore, to capture long-range intra-lane dependencies, we employ a shared lane query to integrally generate offsets and weights for these  $K$  reference points. This design enables each reference point to be updated under global lane information, enhancing lane representation learning through iterative updates.

Given the feature map  $\mathbf{x}$ , the  $l^{\text{th}}$  lane query  $\mathbf{q}_l$  and its reference point  $\mathbf{p}_l$ , we adopt deformable attention mechanism [5] to update query features formulated as:

$$\text{DeformAttn}(\mathbf{q}_l, \mathbf{p}_l, \mathbf{x}) = \sum_{m=1}^M \mathbf{W}_m \left[ \sum_{i=1}^N \sum_{j=1}^K A_{mlij} \cdot \mathbf{W}'_m \mathbf{x}(\mathbf{p}_l + \Delta \mathbf{p}_{mlij}) \right], \quad (3)$$

where  $M$  is the number of attention heads,  $N$  denotes the number of offset locations per sampled point, and  $K$  is the number of sampled points along each curve.  $A_{mlij}$  and  $\Delta \mathbf{p}_{mlij}$  denote the attentions weights and sampling offset, respectively, for the  $i^{\text{th}}$  offset of the  $j^{\text{th}}$  sampled points along the curve in the  $m^{\text{th}}$  attention head.

Unlike BézierFormer [42], which projects sampled points onto image feature maps and performs `grid_sample` to generate  $N_{\text{ref}}$  point queries—each undergoing separate deformable cross-attention—our approach is simpler and more effective. By leveraging global lane information, our method refines local feature aggregation, enhancing the modeling of long-range intra-lane dependencies. Besides, unlike BeMapNet [27], which represents each map element with multiple Bézier curves, our approach maintains efficiency and accuracy by using a single Bézier curve per lane. We also conduct comparative experiments against these two methods (see *Supp. Tab. 4*), showing that our method achieves better modeling capability for lane structures.

### 3.3 Geometry-Enhanced L2L Reasoning

We propose a geometry-enhanced L2L topology reasoning module that explicitly encodes inter-lane geometric relationships. Given the refined lane features  $\mathbf{Q}_{\text{lane}} \in \mathbb{R}^{N \times C}$  and lane endpoint positions

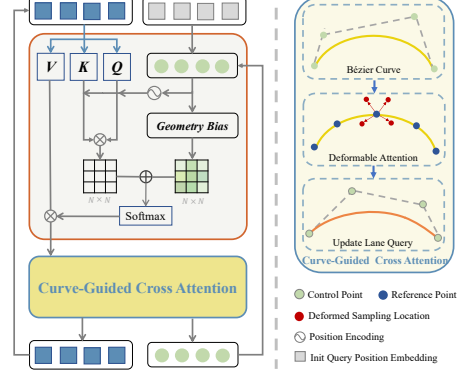


Figure 3: Illustration of our Bézier lane decoder layer, featuring our geometry-biased SA  $\square$  and curve-guided CA  $\square$ .

$\mathbf{P}_{\text{lane}} \in \mathbb{R}^{N \times 2}$ , we construct an L2L relation embedding  $\mathbf{G}_{ll} \in \mathbb{R}^{N \times N \times C}$  by integrating positional embeddings and geometric distance embeddings. Specifically, we first project  $\mathbf{Q}_{\text{lane}}$  into predecessor and successor embeddings using two MLPs and inject positional embeddings  $\mathbf{PE}_{\text{lane}}$  derived from lane endpoints  $\mathbf{P}_{\text{lane}}$ . The L2L relation embedding  $\mathbf{G}_{L2L} \in \mathbb{R}^{N \times N \times C}$  is then constructed as:

$$\mathbf{G}_{L2L} = (\text{MLP}_1(\mathbf{Q}_{\text{lane}}) \odot \text{MLP}_2(\mathbf{Q}_{\text{lane}})) + \mathbf{PE}_{\text{lane}}, \quad (4)$$

where  $\odot$  denotes broadcast concatenation.

To reinforce connectivity relationships, we incorporate geometric distance features as additional cues. Specifically, we compute the end-to-start point distance for each lane pair and embed it into a high-dimensional space using an MLP:

$$\text{DistEmbed}_{L2L}^{i,j} = \text{MLP}(\text{distance}(\mathbf{P}_i^e - \mathbf{P}_j^s)), \quad (5)$$

where  $\mathbf{P}_i^e$  and  $\mathbf{P}_j^s$  denote the endpoint of lane  $i$  and the starting point of lane  $j$ , respectively. These geometric cues are integrated into  $\mathbf{G}_{L2L}$ , which is then processed by an MLP to predict L2L topology:

$$\mathbf{T}_{L2L} = \text{MLP}(\mathbf{G}_{L2L} + \text{DistEmbed}_{L2L}). \quad (6)$$

### 3.4 X-View L2T Reasoning

L2T reasoning requires integrating features from two different perspectives: BEV for lanes and FV for traffic elements. The disparity between these representations poses a challenge for learning spatially consistent relationships. To address this, we introduce a view-aligned fusion module, which aligns BEV-based lane features with spatial and positional information derived from the FV space. Given the predicted 3D lane coordinates  $\mathbf{P}_{\text{lane}}^{3D}$ , we project them onto the FV image to obtain their 2D coordinates  $\mathbf{P}_{\text{lane}}^{2D}$ . Using `grid_sample`, we extract the corresponding FV spatial features  $\mathbf{F}_{\text{lane}}^{2D}$ , which are then integrated with BEV lane queries for enhanced topology reasoning.

To further refine feature alignment, we incorporate positional embeddings to encode the spatial locations of both lanes and traffic elements. The enhanced features are computed as:

$$\tilde{\mathbf{Q}}_{\text{lane}} = \text{MLP}_1(\mathbf{Q}_{\text{lane}}) + \mathbf{F}_{\text{lane}}^{2D} + \mathbf{PE}_{\text{lane}}^{2D}, \quad \tilde{\mathbf{Q}}_{\text{te}} = \text{MLP}_2(\mathbf{Q}_{\text{te}}) + \mathbf{PE}_{\text{te}}^{2D}. \quad (7)$$

The X-view features of lanes and traffic elements are then utilized to construct the L2T relation embedding, denoted as  $\mathbf{G}_{L2T} \in \mathbb{R}^{N \times M \times C}$ , where  $N$  and  $M$  correspond to the number of lanes and traffic elements, respectively. This embedding is generated using the same broadcast concatenation operation applied in the L2L embedding. This approach ensures a consistent representation of spatial relationships between lanes and traffic elements. Finally, we predict the L2T topology by applying an MLP to the combined relation embeddings via:  $\mathbf{T}_{L2T} = \text{MLP}(\mathbf{G}_{L2T})$ .

By bridging the representational gap between BEV and FV, our approach enables robust L2T topology reasoning, effectively capturing spatial relationships between lanes and traffic elements while mitigating the limitations of independent feature fusion.

### 3.5 Loss Functions

#### 3.5.1 Perception Loss

**Lane Loss:** For lane detection, we employ Focal Loss [43] for classification and a combination of point-wise L1 loss and Chamfer distance loss for regression of  $K$  sampling points, ensuring precise lane geometry estimation. **Bounding Box Loss:** For traffic element detection, we use Focal Loss [43] for classification, L1 loss and GIoU loss [44] for bounding box supervision of  $(x, y, w, h)$ .

#### 3.5.2 Topology Learning Losses

Existing methods primarily use Focal Loss for topology classification, focusing on determining connectivity between pairs. However, this approach primarily emphasizes binary classification without explicitly distinguishing the relative importance of connected and non-connected pairs. To better capture topological relationships, we introduce an additional **InfoNCE loss** [45], designed to enhance the discrimination between connected (positive) and non-connected (negative) pairs.

Taking L2T topology as example, we consider  $N$  lane queries and  $M$  traffic element queries from the decoder. Our L2T module generates a relation embedding  $\mathbf{G}_{L2T} \in \mathbb{R}^{N \times M \times C}$ , where each lane query

is associated with every traffic element query, forming an adjacency matrix. Ground truth labels in this matrix are defined as 1 for connected and 0 for non-connected pairs. To strengthen relational learning, we introduce a hard negative mining strategy. Specifically, for each positive pair, we select the top- $n$  hardest negative pairs based on predicted topology scores. This ensures that the model learns to distinguish subtle differences between connected and non-connected pairs. We then apply a symmetric InfoNCE loss<sup>2</sup> as follows:

$$\mathcal{L}_{\text{con}} = -\log \frac{\exp(\mathbf{v}^+)}{\exp(\mathbf{v}^+) + \sum_{\mathbf{v}^-} \exp(\mathbf{v}^-)} = \log \left[ 1 + \sum_{\mathbf{v}^-} \exp(\mathbf{v}^- - \mathbf{v}^+) \right], \quad (8)$$

where  $\mathbf{v}^+$  and  $\mathbf{v}^-$  denote the logits of positive and negative pairs, respectively. To handle multiple positive samples, we extend Eq. (8) following previous works [47, 48]:

$$\mathcal{L}_{\text{con}} = \log \left[ 1 + \sum_{\mathbf{v}^+} \sum_{\mathbf{v}^-} \exp(\mathbf{v}^- - \mathbf{v}^+) \right]. \quad (9)$$

## 4 Experimental Results

### 4.1 Dataset and Metrics

**Dataset.** We evaluate our method on OpenLane-V2 [37], a large-scale dataset specifically designed for topology reasoning in autonomous driving. OpenLane-V2 comprising two subsets: subsetA (derived from Argoverse-V2 [49]) and subsetB (derived from nuScenes [50]).

**Evaluation Metrics.** Following the official evaluation protocol of OpenLane-V2 [37], we utilize  $\text{DET}_l$  and  $\text{DET}_t$  to measure detection accuracy for lanes and traffic elements, respectively. For topology reasoning, we employ  $\text{TOP}_{ll}$  and  $\text{TOP}_{lt}$  to assess Lane-to-Lane and Lane-to-Traffic element relationship prediction. The overall performance is quantified using the OpenLane-V2 Score (OLS):

$$\text{OLS} = \frac{1}{4} [\text{DET}_l + \text{DET}_t + f(\text{TOP}_{ll}) + f(\text{TOP}_{lt})], \quad (10)$$

where  $f$  denotes the square root function. Our evaluations follow the latest version (V2.1.0) of the metrics, as updated in the official OpenLane-V2 GitHub repository<sup>3</sup>.

### 4.2 Implementation Details

**Model Details.** We use a ResNet-50 backbone to extract features, coupled with a pyramid network, FPN, for multi-scale feature learning. Following prior work [3, 1], a BEVFormer encoder [51] with 3 layers is employed to generate a BEV feature map of size  $100 \times 200$ . We employ six decoder layers, using 300 queries for the lane decoder and 100 queries for the traffic element decoder following [2].

**Training Details.** We utilize the AdamW optimizer [52] for model training, with a weight decay of 0.01 and an initial learning rate of  $2.0 \times 10^{-4}$ , which decays following a cosine annealing schedule. Training is conducted for 24 epochs using a total batch size of 8 on 8 NVIDIA 4090 GPUs. Input images are resized to  $1024 \times 800$ , following [2]. The overall training loss is provided in the *Supp.*

### 4.3 Main Results

We compare our model against SOTA methods on the OpenLane-V2 dataset, with results presented in Tab. 1. For subsetA, Our method achieves the highest OLS of 48.9% on subsetA, surpassing all previous methods by a significant margin. Despite utilizing the same traffic head decoder as previous methods [2], our model improves  $\text{DET}_t$  by 0.4, demonstrating its ability to enhance traffic element detection via joint relation-enhanced modeling. Furthermore,  $\text{DET}_l$  achieves a substantial improvement of +3.1, underscoring the effectiveness of our method in enhancing lane detection. Most importantly, we observe notable gains in topology reasoning accuracy, with  $\text{TOP}_{ll}$  and  $\text{TOP}_{lt}$  improving by +5.3 and +4.9, respectively. These results validate the effectiveness of our proposed L2L and L2T topology reasoning modules, which enhance relational reasoning in complex driving

<sup>2</sup>Following the formulation as CLIP [46], the loss is computed bidirectionally within the  $N \times M$  matrix.

<sup>3</sup><https://github.com/OpenDriveLab/OpenLane-V2/issues/76>

Table 1: **Performance comparison with state-of-the-art methods** on the OpenLane-V2 subsetA and subsetB dataset under the latest V2.1.0 evaluation metrics. Results for RoadPainter<sup>‡</sup> are cited from their paper which use old metrics (due to the absence of open-source code or model). TopoMLP<sup>†</sup> results were obtained using their official model, while other results were sourced from the TopoLogic paper. Metrics are reported for detection accuracy (DET<sub>l</sub> and DET<sub>t</sub>) and topology reasoning accuracy (TOP<sub>ll</sub> and TOP<sub>lt</sub>), with overall score (OLS) indicating aggregate performance. Higher values indicate better performance across all metrics. Our method achieves the SOTA performance.

Subset	Method	Venue	Backbone	Epoch	DET <sub>l</sub> ↑	DET <sub>t</sub> ↑	TOP <sub>ll</sub> ↑	TOP <sub>lt</sub> ↑	OLS ↑
setA	VectorMapNet	ICML2023	ResNet-50	24	11.1	41.7	2.7	9.2	24.9
	MapTR	ICLR2023	ResNet-50	24	17.7	43.5	5.9	15.1	31.0
	TopoNet	Arxiv2023	ResNet-50	24	28.6	48.6	10.9	23.8	39.8
	TopoMLP <sup>†</sup>	ICLR2024	ResNet-50	24	28.5	<u>50.5</u>	21.7	<u>27.3</u>	<u>44.5</u>
	RoadPainter <sup>‡</sup>	ECCV2024	ResNet-50	24	<u>30.7</u>	47.7	7.9	24.3	38.9
	TopoLogic	NeurIPS2024	ResNet-50	24	29.9	47.2	<u>23.9</u>	25.4	44.1
	Ours	-	ResNet-50	24	<b>33.8</b>	<b>50.9</b>	<b>29.2</b>	<b>32.2</b>	<b>48.9</b>
	<i>Improvement</i>	-	-	-	3.1 ↑	0.4 ↑	5.3 ↑	4.9 ↑	4.4 ↑
setB	TopoNet	Arxiv2023	ResNet-50	24	24.3	55.0	6.7	16.7	36.8
	TopoMLP <sup>†</sup>	ICLR2024	ResNet-50	24	26.0	<u>58.2</u>	21.0	<u>19.8</u>	<u>43.6</u>
	RoadPainter <sup>‡</sup>	ECCV2024	ResNet-50	24	<u>28.7</u>	54.8	8.5	17.2	38.5
	TopoLogic	NeurIPS2024	ResNet-50	24	25.9	54.7	<u>21.6</u>	17.9	42.3
	Ours	-	ResNet-50	24	<b>32.6</b>	<b>58.8</b>	<b>31.8</b>	<b>25.8</b>	<b>49.7</b>
	<i>Improvement</i>	-	-	-	3.9 ↑	0.6 ↑	10.2 ↑	6.0 ↑	6.1 ↑

scenarios. For subsetB, our RelTopo achieves consistent improvements across all metrics, surpassing previous methods with +3.9 DET<sub>l</sub>, +0.6 DET<sub>t</sub>, +10.2 TOP<sub>ll</sub>, +6.0 TOP<sub>lt</sub>, and an overall +6.1 OLS gain. These results highlight the superiority of our method, which establishes new state-of-the-art on both OpenLane-V2 SubsetA and SubsetB. To demonstrate the effectiveness of our method, we present **qualitative results** in Fig. 4, showing more accurate lane predictions and well-aligned connection points in complex driving environments. Additional visualizations are available in *Supp.*

#### 4.4 Ablation Studies

To provide a thorough evaluation of our method, we conduct extensive studies and analysis. Due to page limitations, additional results and discussions are provided in the *Supp.*, including: **1)** a comparative study of our SA and L2L relation embedding against previous method in [3]; and **2)** an exploration of alternative Bézier representations. Below, we present our main ablations on OpenLane-V2 subsetA, validating the effectiveness of our proposed components. Our baseline model (#1) is built using a deformable-DETR decoder as [2] with lightweight MLP-based topology heads.

Table 2: **Ablation study on key components:** 1) Geometry-Biased Self-Attention (SA) and Curve-Guided Cross-Attention (CA); 2) our L2L and L2T heads; and 3) our proposed contrastive learning.

#L	SA	CA	L2L	L2T	NCE	DET <sub>l</sub>	DET <sub>t</sub>	TOP <sub>ll</sub>	TOP <sub>lt</sub>	OLS
#1						27.7	50.1	21.8	28.4	44.5
#2	✓					28.1	48.8	24.7	28.3	44.9
#3	✓	✓				32.7	50.1	26.8	29.9	47.3
#4	✓	✓	✓			33.7	48.0	28.5	29.7	47.4
#5	✓	✓		✓		33.5	48.4	26.4	31.4	47.4
#6	✓	✓	✓	✓		33.9	50.3	28.6	30.6	48.2
#7	✓	✓	✓	✓	✓	33.8	50.9	29.2	32.2	48.9

**Effect of Relation-Aware Lane Decoder.** Our relation-aware lane decoder consists of two core components: Geometry-Biased Self-Attention (SA) and Curve-Guided Cross-Attention (CA). We progressively integrate these components to examine their impact. **1. Geometry-Biased Self-Attention (SA):** We first replace the standard self-attention [53] in our baseline (#1) with our SA, resulting in model (#2). As shown in Tab. 2, SA enhances lane representation learning, improving TOP<sub>ll</sub> by +2.9. This highlights the benefit of explicitly encoding inter-lane geometric relationships. Besides, we compare our geometry encoding with the distance topology method from Topologic in *Supp. Tab. 3*, further validating the advantages of our method. **2. Curve-Guided Cross-Attention (CA):** Building on model (#2), we introduce Curve-Guided Cross-Attention (CA), forming model (#3). This helps capture global contextual information through sampled points, under lane curve formulation guidance. As shown in Tab. 2, CA boosts DET<sub>l</sub> by +4.6, demonstrating its effectiveness in feature aggregation and

capturing long-range dependencies. **Overall**, integrating both our SA and CA (#3) leads to significant improvements over the baseline (#1), with a +5.0 increase in  $DET_l$ , +5.0  $TOP_{ll}$ , +1.5  $TOP_{lt}$  and an overall +2.8 gain in OLS, which confirm the combined benefits of our relation-aware design.

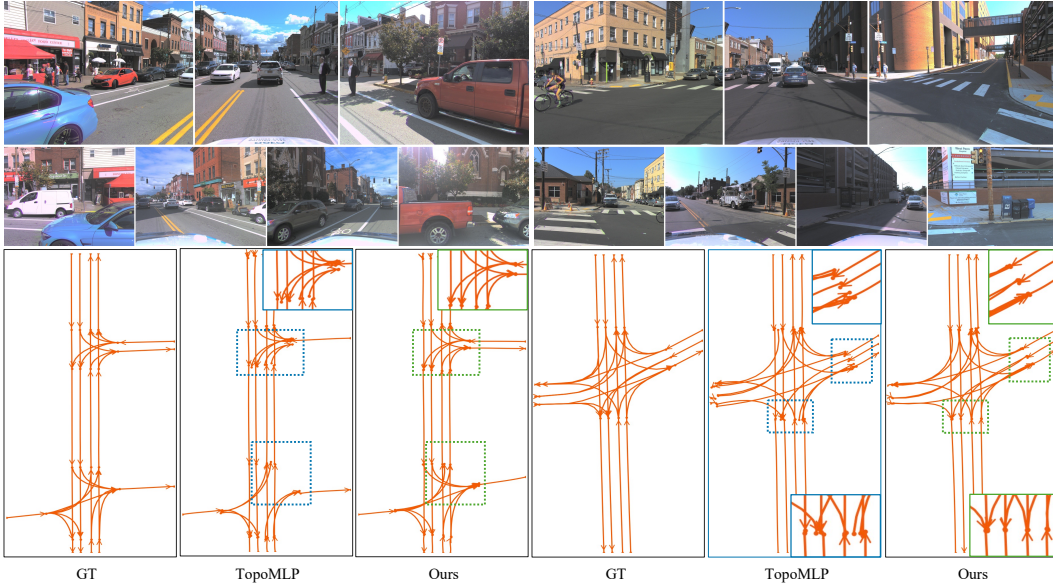


Figure 4: Comparative visual results on OpenLane-V2 subsetA. The top row shows multi-view input images, the bottom row shows lane predictions. We show comparison between groundtruth, TopoMLP [2] and ours. The blue box highlights misaligned connection point predictions from TopoMLP [2], and the green box shows the corresponding aligned predictions from our RelTopo. For clarity, zoomed-in views of selected regions are displayed at the top-right or bottom-right corners.

**Effect of Topology Heads.** To assess our topology heads, we perform a series of ablations by replacing them with counterparts from TopoMLP and present the results in Tab. 2. **1) L2L Head:** Comparing #3 (without our L2L) and #4 (with our L2L), our geometry-enhanced L2L head improves  $TOP_{ll}$  by +1.7 and  $DET_t$  +1.0, validating its effectiveness in capturing L2L relationships, which could in-turn help perception. **2) L2T Head:** Replacing the baseline L2T head (#3) with our proposed head (#5) leads to a +1.5 gain in  $TOP_{lt}$ , confirming its ability to capture L2T relationships. **3) Combined Effect:** Integrating both our L2L and L2T heads (#6) into #3 further enhances topology reasoning, achieving +1.8 in  $TOP_{ll}$ , +0.7 in  $TOP_{lt}$ , and +0.9 in OLS. These results highlights the complementary nature of the two heads, jointly contributing to more accurate detection and reasoning.

**Effect of Contrastive Learning:** Finally, we incorporate our InfoNCE loss for additional supervision in topology learning. Compared to #6, adding InfoNCE loss (#7) improves  $TOP_{ll}$  by +0.6 and  $TOP_{lt}$  by +1.6. demonstrating its effectiveness in enhancing relational understanding.

## 5 Limitations and Future Directions

While our recognition-based topology reasoning framework demonstrates strong performance, it currently lacks interpretability. Future work could explore integrating large language models (LLMs) to enhance relational reasoning between traffic elements and lanes, incorporating traffic rules for improved driving scene understanding. Additionally, incorporating sequential input images or temporal information may enable the model to better capture contextual and dynamic cues, akin to how humans leverage visual memory and temporal continuity in complex driving situations.

## 6 Conclusion

In this work, we present RelTopo, which advances relational modeling for lane perception and topology reasoning. To investigate the impact of relation modeling on perception and reasoning tasks, we conduct extensive experiments and analyses. Our relation-aware lane decoder, featuring geometry-biased self-attention and curve-guided cross-attention, effectively captures structural relationships

among lanes, enhancing lane representation. For topology reasoning, RelTopo incorporates our L2L for inter-lane relation learning and our L2T module that bridges BEV lanes and FV traffic elements, facilitating robust cross-view understanding. Extensive experiments on the OpenLane-V2 benchmark demonstrate that RelTopo achieves state-of-the-art performance, underscoring the efficacy of our relational modeling approach. We believe RelTopo could lay a solid foundation for future research and potentially inspires further advancements in this area.

## References

- [1] Tianyu Li, Li Chen, Huijie Wang, Yang Li, Jiazhi Yang, Xiangwei Geng, Shengyin Jiang, Yuting Wang, Hang Xu, Chunjing Xu, et al. Graph-based topology reasoning for driving scenes. *arXiv preprint arXiv:2304.05277*, 2023.
- [2] Dongming Wu, Jiahao Chang, Fan Jia, Yingfei Liu, Tiancai Wang, and Jianbing Shen. Topomlp: An simple yet strong pipeline for driving topology reasoning. *arXiv preprint arXiv:2310.06753*, 2023.
- [3] Yanping Fu, Wenbin Liao, Xinyuan Liu, Yike Ma, Feng Dai, Yucheng Zhang, et al. Topologic: An interpretable pipeline for lane topology reasoning on driving scenes. *arXiv preprint arXiv:2405.14747*, 2024.
- [4] Yingfei Liu, Tiancai Wang, Xiangyu Zhang, and Jian Sun. Petr: Position embedding transformation for multi-view 3d object detection. In *European Conference on Computer Vision*, pages 531–548. Springer, 2022.
- [5] Xizhou Zhu, Weijie Su, Lewei Lu, Bin Li, Xiaogang Wang, and Jifeng Dai. Deformable detr: Deformable transformers for end-to-end object detection. *arXiv preprint arXiv:2010.04159*, 2020.
- [6] Zhongxing Ma, Shuang Liang, Yongkun Wen, Weixin Lu, and Guowei Wan. Roadpainter: Points are ideal navigators for topology transformer. *arXiv preprint arXiv:2407.15349*, 2024.
- [7] Chenguang Li, Jia Shi, Ya Wang, and Guangliang Cheng. Reconstruct from top view: A 3d lane detection approach based on geometry structure prior. In *Proceedings of the IEEE/CVF Conference on Computer Vision and Pattern Recognition*, pages 4370–4379, 2022.
- [8] Zhixin Zhang, Yiyuan Zhang, Xiaohan Ding, Fusheng Jin, and Xiangyu Yue. Online vectorized hd map construction using geometry. *arXiv preprint arXiv:2312.03341*, 2023.
- [9] Han Li, Zehao Huang, Zitian Wang, Wenge Rong, Naiyan Wang, and Si Liu. Enhancing 3d lane detection and topology reasoning with 2d lane priors. *arXiv preprint arXiv:2406.03105*, 2024.
- [10] Zhengyang Feng, Shaohua Guo, Xin Tan, Ke Xu, Min Wang, and Lizhuang Ma. Rethinking efficient lane detection via curve modeling. In *Proceedings of the IEEE/CVF Conference on Computer Vision and Pattern Recognition*, pages 17062–17070, 2022.
- [11] Zhirong Wu, Yuanjun Xiong, Stella X Yu, and Dahua Lin. Unsupervised feature learning via non-parametric instance discrimination. In *Proceedings of the IEEE conference on computer vision and pattern recognition*, pages 3733–3742, 2018.
- [12] Kaiming He, Haoqi Fan, Yuxin Wu, Saining Xie, and Ross Girshick. Momentum contrast for unsupervised visual representation learning. In *Proceedings of the IEEE/CVF conference on computer vision and pattern recognition*, pages 9729–9738, 2020.
- [13] Xiao Liu, Fanjin Zhang, Zhenyu Hou, Li Mian, Zhaoyu Wang, Jing Zhang, and Jie Tang. Self-supervised learning: Generative or contrastive. *IEEE transactions on knowledge and data engineering*, 35(1):857–876, 2021.
- [14] Noa Garnett, Rafi Cohen, Tomer Pe’er, Roei Lahav, and Dan Levi. 3d-lanenet: end-to-end 3d multiple lane detection. In *Proceedings of the IEEE/CVF International Conference on Computer Vision*, pages 2921–2930, 2019.

- [15] Yuliang Guo, Guang Chen, Peitao Zhao, Weide Zhang, Jinghao Miao, Jingao Wang, and Tae Eun Choe. Gen-lanenet: A generalized and scalable approach for 3d lane detection. In *Computer Vision—ECCV 2020: 16th European Conference, Glasgow, UK, August 23–28, 2020, Proceedings, Part XXI 16*, pages 666–681. Springer, 2020.
- [16] Netalee Efrat, Max Bluvstein, Shaul Oron, Dan Levi, Noa Garnett, and Bat El Shlomo. 3d-lanenet+: Anchor free lane detection using a semi-local representation. *arXiv preprint arXiv:2011.01535*, 2020.
- [17] Ruijin Liu, Dapeng Chen, Tie Liu, Zhiliang Xiong, and Zejian Yuan. Learning to predict 3d lane shape and camera pose from a single image via geometry constraints. In *Proceedings of the AAAI Conference on Artificial Intelligence*, volume 36, pages 1765–1772, 2022.
- [18] Li Chen, Chonghao Sima, Yang Li, Zehan Zheng, Jiajie Xu, Xiangwei Geng, Hongyang Li, Conghui He, Jianping Shi, Yu Qiao, et al. Persformer: 3d lane detection via perspective transformer and the openlane benchmark. In *European Conference on Computer Vision*, pages 550–567. Springer, 2022.
- [19] Yifeng Bai, Zhirong Chen, Zhangjie Fu, Lang Peng, Pengpeng Liang, and Erkang Cheng. Curveformer: 3d lane detection by curve propagation with curve queries and attention. In *2023 IEEE International Conference on Robotics and Automation (ICRA)*, pages 7062–7068. IEEE, 2023.
- [20] Shaofei Huang, Zhenwei Shen, Zehao Huang, Zi-han Ding, Jiao Dai, Jizhong Han, Naiyan Wang, and Si Liu. Anchor3dlane: Learning to regress 3d anchors for monocular 3d lane detection. In *Proceedings of the IEEE/CVF Conference on Computer Vision and Pattern Recognition*, pages 17451–17460, 2023.
- [21] Yueru Luo, Chaoda Zheng, Xu Yan, Tang Kun, Chao Zheng, Shuguang Cui, and Zhen Li. Latr: 3d lane detection from monocular images with transformer. In *Proceedings of the IEEE/CVF International Conference on Computer Vision*, pages 7941–7952, 2023.
- [22] Nicolas Carion, Francisco Massa, Gabriel Synnaeve, Nicolas Usunier, Alexander Kirillov, and Sergey Zagoruyko. End-to-end object detection with transformers. In *Computer Vision—ECCV 2020: 16th European Conference, Glasgow, UK, August 23–28, 2020, Proceedings, Part I 16*, pages 213–229. Springer, 2020.
- [23] Qi Li, Yue Wang, Yilun Wang, and Hang Zhao. Hdmapnet: An online hd map construction and evaluation framework. In *2022 International Conference on Robotics and Automation (ICRA)*, pages 4628–4634. IEEE, 2022.
- [24] Yicheng Liu, Tianyuan Yuan, Yue Wang, Yilun Wang, and Hang Zhao. Vectormapnet: End-to-end vectorized hd map learning. In *International Conference on Machine Learning*, pages 22352–22369. PMLR, 2023.
- [25] Bencheng Liao, Shaoyu Chen, Xinggang Wang, Tianheng Cheng, Qian Zhang, Wenyu Liu, and Chang Huang. Maptr: Structured modeling and learning for online vectorized hd map construction. *arXiv preprint arXiv:2208.14437*, 2022.
- [26] Bencheng Liao, Shaoyu Chen, Yunchi Zhang, Bo Jiang, Qian Zhang, Wenyu Liu, Chang Huang, and Xinggang Wang. Maptrv2: An end-to-end framework for online vectorized hd map construction. *arXiv preprint arXiv:2308.05736*, 2023.
- [27] Limeng Qiao, Wenjie Ding, Xi Qiu, and Chi Zhang. End-to-end vectorized hd-map construction with piecewise bezier curve. In *Proceedings of the IEEE/CVF Conference on Computer Vision and Pattern Recognition*, pages 13218–13228, 2023.
- [28] Wenjie Ding, Limeng Qiao, Xi Qiu, and Chi Zhang. Pivotnet: Vectorized pivot learning for end-to-end hd map construction. In *Proceedings of the IEEE/CVF International Conference on Computer Vision*, pages 3672–3682, 2023.
- [29] Juyeb Shin, Francois Rameau, Hyeonjun Jeong, and Dongsuk Kum. Instagram: Instance-level graph modeling for vectorized hd map learning. *arXiv preprint arXiv:2301.04470*, 2023.



- [30] Jingyi Yu, Zizhao Zhang, Shengfu Xia, and Jizhang Sang. Scalablemap: Scalable map learning for online long-range vectorized hd map construction. In *Conference on Robot Learning*, pages 2429–2443. PMLR, 2023.
- [31] Yi Zhou, Hui Zhang, Jiaqian Yu, Yifan Yang, Sangil Jung, Seung-In Park, and ByungIn Yoo. Himap: Hybrid representation learning for end-to-end vectorized hd map construction. In *Proceedings of the IEEE/CVF Conference on Computer Vision and Pattern Recognition*, pages 15396–15406, 2024.
- [32] Haotian Hu, Fanyi Wang, Yaonong Wang, Laifeng Hu, Jingwei Xu, and Zhiwang Zhang. Admap: Anti-disturbance framework for reconstructing online vectorized hd map. *arXiv preprint arXiv:2401.13172*, 2024.
- [33] Gongjie Zhang, Jiahao Lin, Shuang Wu, Zhipeng Luo, Yang Xue, Shijian Lu, Zuoguan Wang, et al. Online map vectorization for autonomous driving: A rasterization perspective. *Advances in Neural Information Processing Systems*, 36:31865–31877, 2023.
- [34] Yigit Baran Can, Alexander Liniger, Danda Pani Paudel, and Luc Van Gool. Structured bird’s-eye-view traffic scene understanding from onboard images. In *Proceedings of the IEEE/CVF International Conference on Computer Vision*, pages 15661–15670, 2021.
- [35] Yigit Baran Can, Alexander Liniger, Danda Pani Paudel, and Luc Van Gool. Topology preserving local road network estimation from single onboard camera image. In *Proceedings of the IEEE/CVF Conference on Computer Vision and Pattern Recognition*, pages 17263–17272, 2022.
- [36] Tianyu Li, Peijin Jia, Bangjun Wang, Li Chen, Kun Jiang, Junchi Yan, and Hongyang Li. Laneseget: Map learning with lane segment perception for autonomous driving. *arXiv preprint arXiv:2312.16108*, 2023.
- [37] Huijie Wang, Tianyu Li, Yang Li, Li Chen, Chonghao Sima, Zhenbo Liu, Bangjun Wang, Peijin Jia, Yuting Wang, Shengyin Jiang, et al. Openlane-v2: A topology reasoning benchmark for unified 3d hd mapping. *Advances in Neural Information Processing Systems*, 36, 2024.
- [38] Shilong Liu, Feng Li, Hao Zhang, Xiao Yang, Xianbiao Qi, Hang Su, Jun Zhu, and Lei Zhang. Dab-detr: Dynamic anchor boxes are better queries for detr. *arXiv preprint arXiv:2201.12329*, 2022.
- [39] Hao Zhang, Feng Li, Shilong Liu, Lei Zhang, Hang Su, Jun Zhu, Lionel M Ni, and Heung-Yeung Shum. Dino: Detr with improved denoising anchor boxes for end-to-end object detection. *arXiv preprint arXiv:2203.03605*, 2022.
- [40] Xiuquan Hou, Meiqin Liu, Senlin Zhang, Ping Wei, Badong Chen, and Xuguang Lan. Relation detr: Exploring explicit position relation prior for object detection. In *European Conference on Computer Vision*, pages 89–105. Springer, 2025.
- [41] Muhammet Esat Kalfaoglu, Halil Ibrahim Ozturk, Ozel Kilinc, and Alptekin Temizel. Topobda: Towards bezier deformable attention for road topology understanding. *arXiv preprint arXiv:2412.18951*, 2024.
- [42] Zhiwei Dong, Xi Zhu, Xiya Cao, Ran Ding, Caifa Zhou, Wei Li, Yongliang Wang, and Qiangbo Liu. Bézierformer: A unified architecture for 2d and 3d lane detection. In *2024 IEEE International Conference on Multimedia and Expo (ICME)*, pages 1–6. IEEE, 2024.
- [43] T Lin. Focal loss for dense object detection. *arXiv preprint arXiv:1708.02002*, 2017.
- [44] Hamid Rezatofighi, Nathan Tsoi, JunYoung Gwak, Amir Sadeghian, Ian Reid, and Silvio Savarese. Generalized intersection over union: A metric and a loss for bounding box regression. In *Proceedings of the IEEE/CVF conference on computer vision and pattern recognition*, pages 658–666, 2019.
- [45] Aaron van den Oord, Yazhe Li, and Oriol Vinyals. Representation learning with contrastive predictive coding. *arXiv preprint arXiv:1807.03748*, 2018.

- [46] Alec Radford, Jong Wook Kim, Chris Hallacy, Aditya Ramesh, Gabriel Goh, Sandhini Agarwal, Girish Sastry, Amanda Askell, Pamela Mishkin, Jack Clark, et al. Learning transferable visual models from natural language supervision. In *International conference on machine learning*, pages 8748–8763. PMLR, 2021.
- [47] Junfeng Wu, Qihao Liu, Yi Jiang, Song Bai, Alan Yuille, and Xiang Bai. In defense of online models for video instance segmentation. In *European Conference on Computer Vision*, pages 588–605. Springer, 2022.
- [48] Peiyi Wang, Lei Li, Liang Chen, Feifan Song, Binghuai Lin, Yunbo Cao, Tianyu Liu, and Zhifang Sui. Making large language models better reasoners with alignment. *arXiv preprint arXiv:2309.02144*, 2023.
- [49] Benjamin Wilson, William Qi, Tanmay Agarwal, John Lambert, Jagjeet Singh, Siddhesh Khandelwal, Bowen Pan, Ratnesh Kumar, Andrew Hartnett, Jhony Kaesemodel Pontes, et al. Argoverse 2: Next generation datasets for self-driving perception and forecasting. *arXiv preprint arXiv:2301.00493*, 2023.
- [50] Holger Caesar, Varun Bankiti, Alex H Lang, Sourabh Vora, Venice Erin Liong, Qiang Xu, Anush Krishnan, Yu Pan, Giancarlo Baldan, and Oscar Beijbom. nuscenes: A multimodal dataset for autonomous driving. In *Proceedings of the IEEE/CVF conference on computer vision and pattern recognition*, pages 11621–11631, 2020.
- [51] Zhiqi Li, Wenhai Wang, Hongyang Li, Enze Xie, Chonghao Sima, Tong Lu, Yu Qiao, and Jifeng Dai. Bevformer: Learning bird’s-eye-view representation from multi-camera images via spatiotemporal transformers. In *European conference on computer vision*, pages 1–18. Springer, 2022.
- [52] Ilya Loshchilov and Frank Hutter. Decoupled weight decay regularization. *arXiv preprint arXiv:1711.05101*, 2017.
- [53] A Vaswani. Attention is all you need. *Advances in Neural Information Processing Systems*, 2017.

## Supplementary for RelTopo

### A Overall Optimization Objective

As discussed in the main paper, our training objective comprises detection losses for individual elements and reasoning losses for their relationships. Following prior methods [1, 2, 5], traffic element detection is supervised using a combination of classification loss ( $\lambda_1 = 2$ ), L1 loss ( $\lambda_2 = 5$ ), and IoU loss ( $\lambda_3 = 2$ ). Lane detection is similarly optimized with classification and regression losses. The regression component includes L1 loss on control points and a chamfer distance loss  $L_{\text{BézierCD}}$  computed on sampled on-curve points, introduced in our curve-guided cross-attention. We set the number of sampled points  $K$  to 11. The corresponding weights are  $\lambda_4 = 1.5$  for classification,  $\lambda_5 = 0.05$  for L1 loss, and  $\lambda_6 = 0.02$  for the chamfer distance loss. For topology reasoning, we adopt a focal loss for classification, as in prior work, and introduce a contrastive loss  $\mathcal{L}_{\text{con}}$  to further enhance relational learning. Each contrastive pair includes one positive and three negative samples. The focal and contrastive losses are weighted by  $\lambda_7 = 5$  and  $\lambda_8 = 0.1$ , respectively. The overall loss function is defined as:

$$\mathcal{L}_{\text{all}} = \mathcal{L}_{\text{det}} + \mathcal{L}_{\text{relation}}, \quad (11)$$

$$\mathcal{L}_{\text{det}} = \mathcal{L}_{\text{reg}}^{\text{te}} + \mathcal{L}_{\text{reg}}^{\text{lane}} \quad (12)$$

$$= (\lambda_1 \mathcal{L}_{\text{class}}^{\text{te}} + \lambda_2 \mathcal{L}_{\text{L1}}^{\text{te}} + \lambda_3 \mathcal{L}_{\text{IoU}}^{\text{te}}) + (\lambda_4 \mathcal{L}_{\text{class}}^{\text{lane}} + \lambda_5 \mathcal{L}_{\text{L1}}^{\text{lane}} + \lambda_6 \mathcal{L}_{\text{BézierCD}}), \quad (13)$$

$$\mathcal{L}_{\text{relation}} = \lambda_7 \mathcal{L}_{\text{class}}^{\text{topo}} + \lambda_8 \mathcal{L}_{\text{con}}. \quad (14)$$

Table 3: **Experiments on Geometric Distance Topology (GDT)**. “Topologic – GDT<sub>L2L</sub>”: Inference without GDT<sub>L2L</sub>. TopoLogic<sup>†</sup>: Inference using the hyperparameters learned during their lane representation training. “Ours + GDT<sub>lane</sub>”: Replaces our geometry encoding with TopoLogic’s GDT for lane representation learning. “Ours + GDT<sub>L2L</sub>”: Ensembles our L2L predictions with GDT, same as TopoLogic.

Model	DET <sub>l</sub>	DET <sub>t</sub>	TOP <sub>ll</sub>	TOP <sub>lt</sub>	OLS
Topologic	29.9	47.2	23.9	25.4	44.1
Topologic – GDT <sub>L2L</sub>	29.9	47.2	11.6	25.4	40.4
Topologic <sup>†</sup>	29.9	47.2	23.2	25.4	43.9
Ours	<b>33.8</b>	<b>50.9</b>	<b>29.2</b>	<b>32.2</b>	<b>48.9</b>
Ours + GDT <sub>lane</sub>	32.8	50.0	28.4	30.8	47.9
Ours + GDT <sub>L2L</sub>	33.8	50.9	28.7	32.2	48.7

## B Experiments

### B.1 More Analysis on Geometry Topology.

TopoLogic [3] proposes a geometric distance topology (GDT), which shares certain similarities with our Geometry-Biased Self-Attention and Geometry-Enhanced L2L Topology, but *differs fundamentally in design and effectiveness*.

**Lane Representation Learning.** GDT [3] focuses exclusively on connectivity estimation by computing the end-to-start point distance between lanes and updating representations using an additional GCN block. *In contrast*, our method captures richer spatial cues beyond connectivity, such as inter-lane distances and angular relations. These geometric priors—*e.g.*, parallelism, perpendicularity, and merging—are common in real-world road layouts and intuitively leveraged by humans. We explicitly encode the shortest endpoint distance and angular difference between lanes into high-dimensional relational features, which are further projected as biases in self-attention to enhance both perception and downstream topology reasoning.

**L2L Topology Reasoning.** Our method enhances geometric reasoning by leveraging the fact that annotated connected lanes share overlapping endpoints. We encode these end-to-start distances as high-dimensional embeddings and integrate them directly into the L2L relation features during training, enabling the model to learn from geometric cues in an end-to-end manner. In contrast, TopoLogic [3] computes a scalar topology score for each lane pair (ranging from 0 to 1) based on their GDT, and applies this score to adjust L2L predictions (GDT<sub>L2L</sub>) **only** at inference time. This post-hoc refinement is not incorporated in learning and relies on manually assigned hyperparameters, which may not generalize well across different scenarios. As shown in Tab. 3, this design limits model performance and degrades robustness, further highlighting the advantage of our approach.

To better understand the above discussed differences, we conduct three comparative experiments summarized in Tab. 3, and analyze the results below.

**Exp. 1: GDT vs. Geometry-Biased Self-Attention.** To compare GDT with our proposed geometry-biased self-attention, we replace our geometry encoding with TopoLogic’s end-to-start point distance to construct self-attention bias for lane representation learning. As shown in Tab. 3, this modification leads to noticeable performance degradation in lane detection: DET<sub>l</sub> drops by 1.0 (Ours vs. Ours + GDT<sub>lane</sub>), TOP<sub>ll</sub> decreases by 0.8, and TOP<sub>lt</sub> falls by 1.4. These results suggest that TopoLogic’s GDT is insufficient for capturing the rich inter-lane spatial relationships essential for effective topology reasoning, reaffirming the advantage of our proposed relation embedding.

**Exp. 2: Evaluating GDT in L2L Topology Reasoning.** Unlike our (geometry-enhanced L2L topology) method, which integrates geometric cues directly into the L2L relation embedding during training, TopoLogic treats GDT as an auxiliary component applied at inference time to adjust L2L predictions. This approach relies on several hyperparameters to balance the influence between GDT and model-based predictions. Although these weights are optimized during training as part of lane representation learning, they are not used during L2L inference—manual values are assigned instead.

To examine the effect of GDT on topology learning, we evaluate TopoLogic’s official model under two configurations: 1). TopoLogic<sup>†</sup>: which uses the hyperparameters learned during training; 2)

TopoLogic –  $\text{GDT}_{\text{L2L}}$ : which removes GDT from the L2L topology inference process. As shown in Tab. 3, both configurations lead to significant performance degradation, with a severe drop in L2L topology accuracy when GDT is removed during L2L inference (TopoLogic vs. TopoLogic –  $\text{GDT}_{\text{L2L}}$ ). This suggests that TopoLogic’s lane features alone do not sufficiently encode relational information for effective topology reasoning. The reliance on post-hoc adjustments and manual tuning limits the robustness and generalizability of the method.

**Exp 3: Applying GDT to Our L2L Inference.** We further investigate the generalizability of GDT by incorporating it into our model’s L2L inference, following TopoLogic’s ensembling strategy. Specifically, we fuse our L2L predictions with GDT outputs using their predefined hyperparameters, without modifying our trained model. As shown in Tab. 3, this ensembling leads to a decrease in  $\text{TOP}_{ll}$  by 0.5 (Ours +  $\text{GDT}_{\text{L2L}}$  vs. Ours). This outcome highlights the limited transferability of TopoLogic’s formulation. In contrast, our model achieves strong L2L performance without requiring additional tuning or post-processing, demonstrating that our relation embedding offers a more effective and learnable approach to modeling geometric topology.

Table 4: Comparison with different bézier representation.

Lane Rep.	$\text{DET}_l$	$\text{DET}_t$	$\text{TOP}_{ll}$	$\text{TOP}_{lt}$	OLS
BeMapNet	29.9	50.0	25.9	28.9	46.2
BézierFormer	31.0	49.7	26.1	29.6	46.5
Ours	<b>33.8</b>	<b>50.9</b>	<b>29.2</b>	<b>32.2</b>	<b>48.9</b>

## B.2 Comparison of Bézier representation.

We compare our Bézier-based lane representation with other alternative formulations in ??, BézierFormer uses `grid_sample` to sample features and separately predicts offsets and attention weights for each point within deformable attention, which increases computational overhead and compromises instance-level consistency in lane prediction. In contrast, our method predicts offsets and attention weights jointly for the entire lane instance using a single lane query, resulting in improved efficiency and coherence. BeMapNet employs a piecewise Bézier representation by dynamically predicting the number of segments, which increases model complexity and uncertainty. In the task of lane topology reasoning, such dynamic segmentation does not yield performance gains and lacks the structural regularity that our fixed Bézier formulation provides.

## B.3 Qualitative Results

We present additional qualitative results in Fig. 5 and Fig. 6. Leveraging our proposed components, RelTopo demonstrates superior perception of lane centerlines compared to previous methods, as shown in the second row of the figures. Moreover, RelTopo achieves more accurate lane-to-lane (L2L) and lane-to-traffic-element (L2T) topology reasoning, as illustrated in the last two rows. Notably, RelTopo exhibits significantly improved L2T topology reasoning performance in complex scenarios involving intricate L2T relationships.

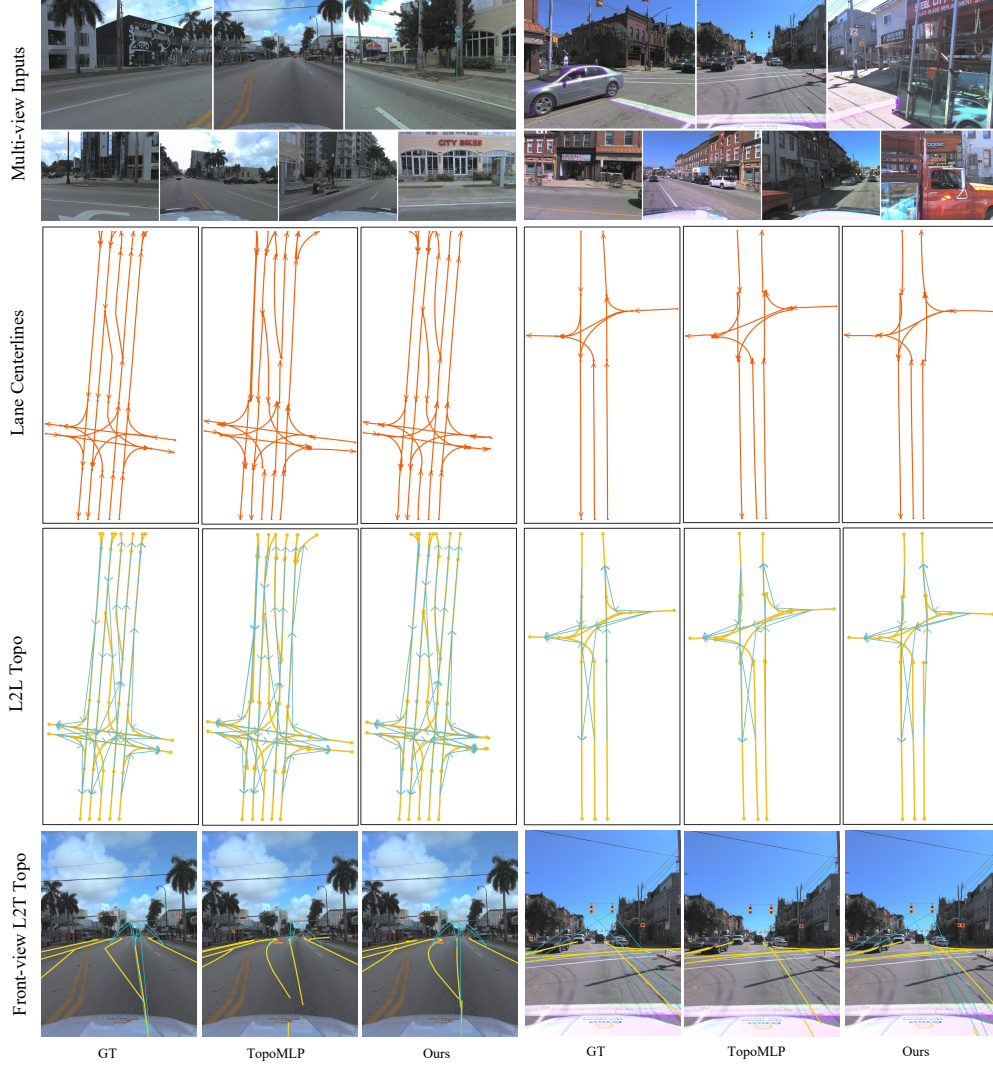


Figure 5: Qualitative results comparison. The 1<sup>st</sup> row presents the multi-view input images, the 2<sup>nd</sup> row shows the predicted lane centerline results, and the 3<sup>rd</sup> row illustrates the predicted L2L topology results, with light blue arrowlines indicating directed connectivity between lanes. The final row depicts the front-view L2T topology predictions, where orange boxes highlight detected traffic elements (*e.g.*, traffic lights and signs), mbevlane lines denote projected lanes, and blue lines represent the pairing relationships between traffic elements and lanes. Each result row consists of three columns: the left column shows ground truth, the center column shows results from TopoMLP, and the right column presents our results. Two data samples are illustrated in this figure.

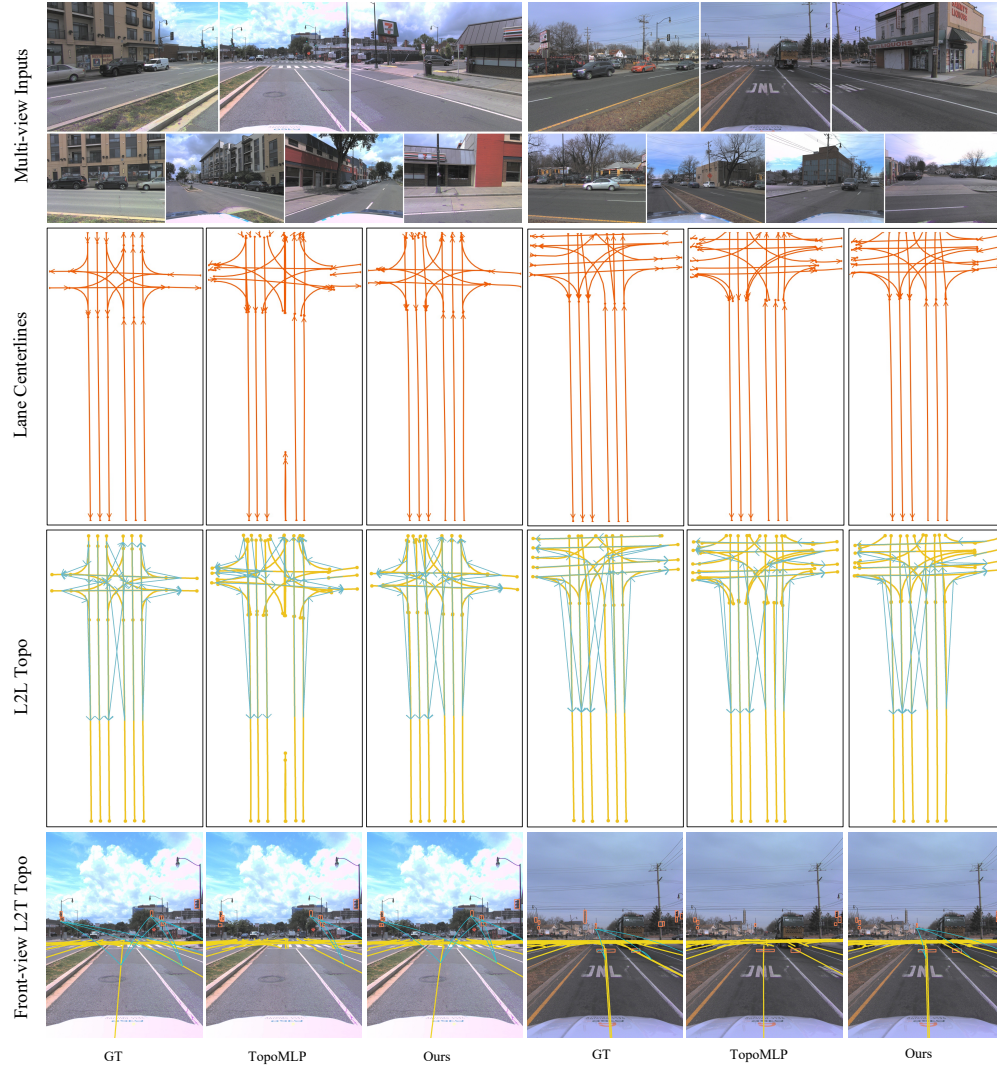


Figure 6: More qualitative result comparison. With our proposed designs, RelTopo achieves more accurate predictions for lane centerlines, as well as L2L and L2T topology reasoning.